# Raman lidar monitoring of extinction and backscattering of African dust layers and dust characterization

*F. De Tomasi, A. Blanco and M. R. Perrone*

*Dipartimento di Fisica, Istituto Nazionale di Fisica della Materia, Universita' di Lecce, 73100 Lecce (Italy)*

## Abstract

Results on the monitoring of strong African dust outbreaks at Lecce in the south-eastern corner of Italy (40° 20' N, 18° 6'E) during May 2001 are presented. This activity has been performed in the framework of the European Aerosol Research Lidar Network (EARLINET). The lidar station of Lecce is located on a flat rural area that is at about 800 km from the northern Africa coast. So, it is closer to Africa than most or all other EARLINET stations and allow monitoring African dust transport early in its life cycle, at all levels in the plume. An elastic-backscatter Raman lidar based on a XeF excimer laser (351 nm) has been used to monitor the time evolution and vertical structure of the dust layers and get independent measurements of the aerosol extinction and backscatter coefficient. The findings are presented in terms of vertical profiles of the extinction and backscatter coefficient, and of the lidar ratio. A quite deep dust layer extending between 2 and 6 km and characterized by a backscatter coefficient of ~0.0016 $(km\ sr)^{-1}$, a lidar ratio of about 50 sr and an aerosol optical depth of 0.26 has been observed on May 17$^{th}$, 2001 between 18:55 and 20:07 UT. The layer persisted for about 5 days. Dust layers of lower optical thickness and shorter persistence time, have generally been monitored at the lidar site during African dust outbreaks. Results on the chemical and morphological characterization of the dust collected at the lidar station are also given to further support the origin of the monitored aerosol layers.

## 1. Introduction

Desert dust particles represent a large fraction (of the order of 30-50%) of the naturally occurring tropospheric aerosols and the scientific community has made great efforts to document and understand the interactions of mineral aerosols (dust) with environment[1-3]. Desert dust absorbs at ultraviolet, visible and infrared wavelengths. Therefore, its presence in the atmosphere can either lead to a cooling or warming effect, depending on properties as single scattering albedo, altitude of the layer and albedo of the underlaying surface[3,4]. Very large quantities of African dust are carried into the Mediterranean basin every year[5] (~ $5 \times 10^8$ ton/yr). The African dust transport is driven by complex wind fields and the vertical structure of the dust layers reflects that complexity[1]. As it has been mentioned, the vertical structure of the dust layers is of peculiar importance to infer their radiative impact and a direct documentation on the vertical structure of the Mediterranean transport of dust is lacking.

This paper presents the first results on the time- and altitude-resolved properties of African dust events observed by a new elastic-backscatter Raman lidar station that is located at the University of Lecce (40º 20' N, 18º 6' E) on the south-eastern corner of Italy. In particular, the lidar is located on a rather flat, rural area that is at about 15 and 25 km from the Adriatic and Ionic Sea, respectively, and at about 800 km from the northern Africa coast. This last peculiarity makes the lidar station of Lecce rather suitable for the monitoring of desert type aerosols advected to Lecce from the African deserts without being significantly affected by anthropogenic aerosols and by the removal of coarse mode particles with diameters >1 μm as a consequence of gravitational setting[6]. Let us mention that elastic-backscatter Raman lidars allow getting independent measurements of the aerosol extinction and backscatter coefficient and therefore provide optical-particle properties on a highly resolved vertical and temporal scale[7]. Several Sahara dust episodes have been monitored during the 2001 year and results on the most severe outbreaks that have occurred during May, 2001 are reported in the paper. The main aim of the paper is to discuss lidar data sets that are representative of severe

Sahara dust events, which provide a direct documentation on the vertical structure of the Mediterranean transport of dust[1] and may contribute to a better understanding of dust outbreaks. The lidar data are presented in conjunction with the air mass back-trajectory analysis performed by the German Weather Service, to better characterize the vertical structure and temporal evolution of the Sahara dust layers. The images provided by the Sea-viewing Wide Field-of-view Sensor (SeaWiFS) that is carried by the SeaStar spacecraft on the NASA EOS-AM platform have also been used to get clear views of the suspended Sahara dust particles over the Mediterranean Sea[8].

Results on the chemical and morphological characterization of the dust samples collected at the lidar station are also given to further support the origin of the monitored aerosol layers. Moreover, there is a clear need to provide information on mineralogical composition needed for dust modeling on global and regional scales.

These studies have been performed as part of the European Project EARLINET[9], whose main goal is to establish a statistical database of the horizontal, vertical, and temporal distribution of aerosols on a continental scale, using a network of 21 lidar stations distributed over Europe**.** It is worth noting that the lidar station of Lecce is closer to Africa than most of all other EARLINET stations. It is also quite isolated from local anthropogenic or soil-derived contamination and therefore is one of the best suited EARLINET stations to monitor African dust transport early in its life cycle, at all levels in the plume.

The experimental structure of the elastic-backscatter Raman lidar besides the analytical techniques applied to determinate the atmospheric parameters are presented in Sec. II. Lidar measurement examples are given in Section III. The techniques used to characterize the chemical and physical properties of the Sahara dust particles besides the corresponding experimental results are reported in Section IV. Section V presents the concluding remarks.

## 2. Lidar set up and analytical equations

Figure 1 shows the layout of the Rayleigh-Raman lidar. A XeF excimer laser (Lambda Physik LPX 210 I) delivering light pulses of 30 ns duration at 351 nm, with a maximum repetition rate of 100 Hz and an energy of up to 250 mJ is used as radiation source. The expanded outgoing laser beam has a cross section of 40 x 25 $mm^2$ and an average divergence of 0.3 mrad. Collection of the backscattered radiation is obtained by a Newtonian telescope, whose primary mirror has 30 cm-diameter and 120 cm-focal length. The backscattered radiation is spatially filtered by a 4 mm field stop aperture (A) located on the telescope focus, is collimated by a 10 cm-focal length lens (L1), and is then monitored in two different channels. An uncoated fused silica plate (Q) allows the splitting of the backscattered radiation into two beams. The light reflected by the plate is used for the measurement of the elastic backscattered radiation at 351 nm. The beam transmitted by the silica plate is instead used to detect the Raman nitrogen signal at 382 nm. A double-grating monochromator Mn (Jobin-Yvon DH10 UV) equipped with a 1 x 8 $mm^2$ slits and characterized by an out of band rejection better than $10^{-8}$, is used in each channel to spectrally resolve the back-scattered radiation. No cross talk between nearby lines has been observed. The back-scattered radiation is focused on the entrance slit of each monochromator by a 7.5 cm-focal length lens (L). The nitrogen Raman signal monitored by a photosensor (Ph), is detected in photon-counting regime by using a 300 MHz discriminator (Phillips Scientific Mod. 6908) and a multichannel scaler (EG&G MCS-Mod. 914 P). The elastic signal monitored by a photosensor is acquired in both the analog-to-digital (A/D) and photon-counting modes. A LeCroy oscilloscope (Mod. 9361/C-300MHz) is used for the A/D acquisition. Neutral density filters (F) in front of the monochromator are required for the elastic and $N_2$ Raman signals to reduce count rates. The multichannel scaler operates with a dwell time of 100 ns, yielding a spatial resolution of 15 m, even if its minimum dwell time is 5 ns. The system is fully remote controlled by locally-developed software.

Let us recall the main relations we have used to retrieve extinction and backscatter coefficients, and lidar ratio values. The determination of the aerosol backscatter coefficient is based on the elastic and Raman signals when the combined lidar technique is used and it is given by the following relation according to Ansmann et al.[7]:

$$\beta_{\lambda_0}^{aer}(z) = \{[\beta_{\lambda_0}^{aer}(z_0) + \beta_{\lambda_0}^{mol}(z_0)] \times \frac{P_{N_2}(z_0) P_{\lambda_0}(z) N_{N_2}(z)}{P_{\lambda_0}(z_0) P_{N_2}(z) N_{N_2}(z_0)} \times \Delta T_R(z, z_0)\} - \beta_{\lambda_0}^{mol}(z) \qquad (1)$$

where $\beta_{\lambda_0}^{mol}(z)$ and $\beta_{\lambda_0}^{aer}(z)$ denote the backscatter coefficient for molecular and particle scattering, respectively. $P_{\lambda o}$ $(z)$ denotes the return signal from distance $z$ at the XeF laser wavelength $\lambda_o$, $P_{N2}(z)$ is the Raman nitrogen return signal from distance $z$.. $N_{N2}(z)$ is the nitrogen number density at distance $z$. The reference height $z_0$ is usually chosen such that $\beta_{\lambda_0}^{aer}(z_0) + \beta_{\lambda_0}^{mol}(z_0) \cong \beta_{\lambda_0}^{mol}(z_0)$. These clear air conditions normally prevail in the upper troposphere[10]. The transmission correction function is given by

$$\Delta T_R(z, z_0) = \frac{\exp\left\{-\int_{z_0}^{z} \left[\alpha_{N_2}^{aer}(\zeta) + \alpha_{N_2}^{mol}(\zeta)\right] d\zeta\right\}}{\exp\left\{-\int_{z_0}^{z} \left[\alpha_{\lambda_0}^{aer}(\zeta) + \alpha_{\lambda_0}^{mol}(\zeta)\right] d\zeta\right\}}. \qquad (2)$$

where $\alpha_x^{mol}$ and $\alpha_x^{aer}$ denote the extinction of light at the wavelength $\lambda_x$ of the $x$ species, by atmospheric gas molecules and aerosol particles, respectively. Radiosonde data of pressure and temperature are used to calculate air density profiles and the reduction in transmission due to molecular scattering. Radiosonde measurements are performed every six hours, by the Italian weather service at the meteorological station of Brindisi (40° 39’ N, 15° 57’ E) that is located about 40 km north-west from the lidar site.

The particle extinction coefficient is determined from the measured nitrogen Raman signal and it is given by

$$\alpha_{\lambda_0}^{aer}(z) = \frac{d/dz\{\ln[N_2(z)/P_{N_2}(z)z^2]\} - \alpha_{\lambda_0}^{mol}(z) - \alpha_{N_2}^{mol}(z)}{1 + (\lambda_0/\lambda_{N_2})^k} \qquad (3)$$

$\lambda^{-k}$ describes the wavelength dependence of the aerosol extinction, where the Angstrom coefficient $k$ is a parameter which has to be guessed since it depends on the aerosol size and composition[11, 12] . $k$ =1 is assumed for aerosol particles whose dimensions are of the same order of magnitude as the measurement wavelength. Whereas, $k$ =0 is more appropriate for large particles[7]. We have taken $k$=1 since this value is normally assumed[12] between 351 nm and 383 nm. From an analytic calculation, the error in the derived aerosol extinction at 351 nm is about 5% if $k$ varies between 0 and 2 when an assumed value $k$=1 is used. In the same conditions, the maximum relative error on β due to the uncertainty on $k$ is calculated to be of the order of 0.1 multiplied the optical thickness between $z$ and $z_0$, thus it will be less than 5% for the cases reported in the paper.

The independent determination of the particle extinction and backscatter coefficient implies, in addition, the determination of the extinction-to-backscatter ratio (lidar ratio):

$$S(z) = \alpha_{\lambda o}^{aer}(z) / \beta_{\lambda_0}^{aer}(z) \qquad (4)$$

Let us mention that under our experimental conditions, the combined elastic-backscatter Raman technique can only be applied to measurements performed after sunset, because the weak inelastic backscatter signal can be detected only in absence of strong daylight background. The so-called Klett method[13] based on the assumption of a lidar ratio profile, is used to retrieve the aerosol backscatter coefficient from day-time lidar measurements.

In the data analysis it is assumed that the overlap function is unity at altitudes $z \geq 500$ m. This assumption is also supported by the results on the intercomparison campaign performed within the EARLINET project[14].

## 3. Lidar measurements and discussion

The lidar measurements have been performed under the so-called ”dust alerts” issued by the Atmospheric Modeling Weather Forecasting Group of the University of Athens, Grecee (http://forecast.uoa.gr/forecastnew.html), and the results on two severe African dust outbreaks monitored on May 2001 are reported in this paper. Dust layers characterized by a quite different vertical structure and temporal evolution have been monitored during the two events. The first Sahara dust event has been observed between May 3rd and May 5th. The second one has been observed between May 17th and May 21st.

### *3a. Dust event of May 3-5, 2001*

The four-day analytical back trajectories of May 3rd at 13:00 UT are shown on Fig.2. The atmospheric backward trajectories have been calculated on a 3-dimensional grid with a time resolution of six hours, by the German Weather Service from the wind fields of the European numerical weather prediction model[15]. It is believed that this calculation method leads to lower uncertainties in comparison to those of other methods, e.g. isentropic calculation. The accuracy of the calculated trajectories depends on the synoptic conditions. The higher the wind speed the lower the uncertainty of the trajectories. Usually the deviation between the calculated and the actual track of an air parcel is about 10% to 20% of the trajectory length for the trajectories used in this study[16]. The data are provided for six distinct arrival height levels (975, 850, 700, 500, and 200 hPa) and for two arrival times (13:00 UT and 19:00 UT) on a day-by-day basis.

The back trajectories of May 3rd (Fig.2) indicate that air masses coming from East Europe are sampled over the lidar station of Lecce at altitude lower than about 3 km. By contrast, air masses coming from the North-West of Africa are sampled at altitude above 3 km from ground. This dust episode has also been observed by the lidar station[17] at Potenza (40° 36' N, 15° 44' E) and Athens (37° 58' N, 23° 47' E). Both lidar stations partecipate to the EARLINET Project. Moreover, the satellite SeaWiFS image taken on May 4th that is shown in Fig. 3 (http:seawifs.gsfc.nasa.gov/cgibrs/seawifs_subreg.pl), clearly shows the presence of Saharan dust layers over the Eastern Mediterranean Sea.

Figure 4 shows the vertical structure of the aerosol backscatter coefficient $\beta_{\lambda_0}^{aer}$ that has been retrieved from lidar measurements performed at different hours of the day, on May (a) 3rd and (b) 4th. The vertical profiles of $\beta_{\lambda_0}^{aer}$ referring to measurements performed before the sun set time (~19:00 UT) have been retrieved by the Klett method, assuming a lidar ratio value equal to 50 sr. The time (UT) during which the measurements have been performed is reported on the right side of each profile. The repetition rate of the laser was 80 Hz. A measurement is composed of single acquisitions of 2-4 minutes. The single acquisitions of the elastic and Raman (if available) signals have been first averaged if no significant evolution was noticed and have then been used to calculate the backscatter coefficient according to Eq. (1) or to the Klett method[13]. Vertical averaging has then been applied to $\beta_{\lambda_0}^{aer}(z)$. The window length was 60 m up to about 6 km and 120 m at larger altitudes. The reference height $z_0$ has been located at an altitude between 7 and 10 km during cloud-free conditions and for the backscatter coefficient boundary value, $\beta_{\lambda_0}^{aer}(z_0) = 0$ has been chosen. The following technique has been used to calibrate to zero the backscatter coefficient. A simulated molecular lidar signal has been first calculated from radiosounding data both for the elastic and the Raman channel. Then, at altitudes between 7 and 12 km, a spatial interval 1-2 km long where the experimental elastic (Raman) lidar signal could be matched by the simulated elastic (Raman) signal has been determined. In these intervals the experimental signals can thus be fitted by the simulated signals, and the result of the fit is used to replace the experimental signal in the chosen interval. We believe this procedure reduces the errors associated to the statistical noise affecting the experimental signal at the calibration altitude. The statistical uncertainties on the retrieved $\beta_{\lambda_0}^{aer}(z)$ values have been calculated from the law of error propagation by assuming a Poisson noise on the lidar signals and it has been found that they are within 1-20% up to about 6 km for $\beta_{\lambda_0}^{aer}(z) > 0.0005$ (km-sr) $^{-1}$. Typical examples of the backscatter coefficient profiles with the statistical errors are shown on Figs. 5, 6 and 10. The relative error on the total backscatter coefficient due to the uncertainty of the particle reference value $\beta_{\lambda_0}^{aer}(z_0)$ is equal to the relative error on the total backscattering at the calibration altitude; this means that the relative error on $\beta_{\lambda_0}^{aer}(z)$ is lower than 10% if the error of $\beta_{\lambda_0}^{aer}(z_0)/\beta_{\lambda_0}^{mol}(z_0)$ is lower than 0.01 and $\beta_{\lambda_0}^{aer}(z)/\beta_{\lambda_0}^{mol}(z)$ is larger than 0.1. It has been shown[18] for mid latitudes and $\lambda_0$ = 308 nm that $\beta_{\lambda_0}^{aer}(z_0)/\beta_{\lambda_0}^{mol}(z_0) \leq 0.01$ under typical air conditions for the upper troposphere.

The larger values of the backscatter coefficient that one observes on the first profile on the left of Fig. 4a, at altitudes between 4 and 5 km, can be ascribed to the presence of an African dust layer, in accordance to the back trajectories of Fig. 2. By contrast, we believe that the vertical structure of $\beta_{\lambda_0}^{aer}$ at altitudes lower than 3.5 km, is determined by local aerosols and by the air masses coming over the lidar station from Eastern Europe. Therefore, the data of Fig. 4a at altitudes larger than 3 km, show the evolution of the vertical structure of the dust layer on May 3$^{rd}$. One observes that the layer thickness that was about 1 km in the early day hours increases to about 3 km after midday. This vertical structure evolves during the day, in such a way that two maxima have been monitored between 14:00 and 14:44 UT: a broad one between 3 and 5 km and one between 5 and 6 km. By contrast, a layer extending between 3.5 and 6.2 km is observed in the time interval 22:44-23:28 UT. The peak value of the backscatter coefficient that was about 0.001 (km sr)$^{-1}$ in the early hours of May 3$^{rd}$, increases up to about 0.0025 $(km\ sr)^{-1}$ during the following hours. Figure 5 shows the vertical profiles of the (a) backscatter and (b) extinction coefficients and (c) of the lidar ratio that have been retrieved from measurements started on May 3rd at 23:40 UT and ended on May 4th at 01:00 UT. The independent lidar retrievals of the extinction and backscatter coefficients allow a better characterization of the aerosol properties[6, 19-22]. The extinction-to-backscatter ratio depends on the size distribution and optical properties of the particles. It generally increases with decreasing particle size and increasing contribution of absorption to light extinction[6,19].

The time averaged nitrogen Raman signals have been used to calculate the extinction coefficient according to Eq. (3). Retrievals of aerosol extinction profiles are limited to altitudes > 500 m where the overlap function is unity. The extinction is calculated by a linear fit of the quantity under derivative in Eq. 3 in an altitude interval of typically 150 m below 1-2 km and 400 m above. The uncertainty in the extinction is calculated by the uncertainty of the slope of the fitting straight line. The sharp decrease of the error bars that can be observed in the extinction vertical profiles at larger heights is caused by the larger fitting interval. The profiles of $S(z)$ have been computed using the aerosol extinction and backscatter profiles, and therefore the aerosol backscatter profiles have been smoothed to match the resolution of the aerosol extinction profiles before computing $S(z)$. The vertical structure of $\beta_{\lambda_0}^{aer}(z)$, $\alpha_{\lambda o}^{aer}(z)$, and $S(z)$ of Fig. 5 reveals that aerosol layers characterized by different extinction and lidar ratio values and maybe of different origin and type are located at different altitudes, in accordance to the analytical back trajectories of Fig. 2. The aerosol layering may also be supported by the vertical structure of the potential temperature profile that has been obtained from radiosonde measurements performed at Brindisi on May 3rd at 23:00 UT and, that is shown in Fig. 5a (full dots). In fact, Fig. 5a reveals that the potential temperature increases with altitude. An aerosol layer characterized by a lidar ratio about 23 sr is located between 0.8 and 1.5 km. By contrast, a deeper layer characterized by an average lidar ratio value of 57 sr, extends between 3 and 6 km. Lidar ratios ranging from 51 to 57 sr have been assumed by

Sasano and Browell[23] to get trustworthy backscatter profiles at 300 nm, from measurements in lofted Saharan dust layers near Barbados. By contrast, unexpectedly large lidar ratios, mainly between 60 and 100 sr at 355 nm and, between 40 and 75 sr at 532 nm, have recently been observed in dust layers by Mattis et al.[6] over Leipzig (Germany). The long-range transport that leads to an efficient removal of coarse mode particles with diameters >1μm by gravitational settling and the non-spherical shape of the particles have been considered responsible for the large Saharan dust lidar ratio values. To this end it is worth mentioning that the numerical model developed by Barnaba and Gobbi[24] has provided lidar ratio values ranging from 35 to 50 sr at 500 nm for nonspherical dust aerosols. Lidar ratios ranging from 20 to 25 sr at 532 nm and from 42 to 47 sr at 355 nm, have instead been obtained for desert aerosols from the numerical study based on the Mie theory that has been performed by Ackermann[25]. We believe that the above comments further support the Sahara origin of the layer located between 3 and 6 km in all the profiles of Fig. 4a and 5. The aerosol optical thickness (AOT) of the dust layer of Fig. 5 that has been computed by integrating the aerosol extinction coefficient between 3 and 6 km, is 0.21.

Let us mention that the four-day analytical back trajectories provided by the German Weather Service for May 4$^{th}$ and 5$^{th}$ are quite similar to those of Fig. 2. As a consequence one observes from Fig. 4b that the vertical structure of the aerosol backscatter coefficient is quite similar to that of May 3$^{rd}$ and it undergoes few modifications during all day. Indeed, the dust layer characterized by a peak $\beta_{\lambda_0}^{aer}$ value of about 0.002 (km sr)$^{-1}$, which is located between 2.8 and 6 km in the early hours of the day, extends from about 3.5 km to 6.5 km at midday and then, from about 3 km to 6 km at night. It appears from Fig. 4 that a rather stable stratification of the lowermost troposphere prohibited the mixing of the Sahara dust plume with the continental and marine aerosols located below 3 km altitude. This assertion may also be supported by the potential temperature vertical profile obtained from the radiosonde measurements taken at Brindisi on May 4$^{th}$ at 23:00 UT and that is shown in Fig. 6a (dots).

An inversion layer located in the interval 0-2.5 km is shown by Fig. 6a (dots). By contrast a nearly adiabatic potential temperature profile that is typical of mixed layers extends from 2.5 to 4.7 km. Figure 6 shows the vertical profiles of the (a) backscatter and (b) extinction coefficient and (c) of the lidar ratio that have been retrieved from measurements performed on May 4th from 22:00 to 23:00 UT. The spatial distribution of $\beta_{\lambda_0}^{aer}(z)$, $\alpha_{\lambda o}^{aer}(z)$, and $S(z)$ is similar to that of Fig. 5. An aerosol layer with a quite low extinction coefficient and an average lidar ratio of 20 sr, extends between 0.7 and 2 km. By contrast, a deeper layer characterized by an average lidar ratio value of 53 sr, extends between 2.7 and 5.4 km. The AOT of this last layer is 0.22. Finally, let us mention that the presence of low altitude clouds has not allowed us to get on May 5th, backscatter coefficient profiles with a high signal to noise ratio.

*3b. Dust event of May 17-21, 2001*

The last Sahara dust event studied in the paper, has been observed between May 17th and May 21st. The four-day analytical backtrajectories of May 17th at 19:00 UT (Fig. 7) indicate that Northern Africa is the source of all air masses sampled at altitudes above few hundred meters from ground. Let us mention that the four-day analytical back trajectories provided by the German Weather Service for May 18th, 19th, 20th and 21st are quite similar to those of Fig. 7. This last Sahara dust outbreak has also been observed by the EARLINET lidar stations[17] at Potenza, Italy (40° 36' N, 15° 44' E), Naples, Italy (40° 50' N, 14° 11' E), Thesaloniki, Greece (40° 30' N, 22° 54' E), Athens, Greece (37° 58' N, 23° 47' E), Barcelona, Spain (41° 23' N, 2° 07' E), Palaiseau, France (48° 43' N, 2° 14' E), Neuchatel, Swiss (46° 59' N, 6° 57' E), and Garmisch-Partenkirchen, Germany (47° 28' N, 11° 04' E). The satellite SeaWiFS image of May 18th (Fig. 8) may further confirms the presence of an Africa dust plume above the lidar station of Lecce. In fact, Fig. 8 reveals the presence of deep Saharan dust layers over the Eastern Mediterranean Sea and along the costs of Southern Italy, and Greece, even if Italy is hidden by clouds.

Figure 9 shows the vertical profiles of the aerosol backscatter coefficient retrieved from lidar measurements performed between May 17th and May 21st. The day and time (UT) during which the measurements have been performed, are reported on the right side of each profile. The presence of a rather persistent aerosol layer between about 1 and 6 km is revealed by the measurements of Fig. 9. The quite large values of $\beta_{\lambda_0}^{aer}$ that one observes on the profiles of May 19th and 21st at altitudes larger than 4.5 km, are determined by the presence of clouds. Therefore, we believe that a dust layer of thickness ranging between 4 and 5 km has been monitored at heights above 1 km, during the last African dust event. Figure 10 shows the vertical profiles of the (a) backscatter and (b) extinction coefficient, and (c) of the lidar ratio that have been retrieved from measurements performed on May 17th between 18:55-20:07 UT. The vertical structure of $\beta_{\lambda_0}^{aer}(z)$, $\alpha_{\lambda o}^{aer}(z)$, and $S(z)$ reveals the presence of different aerosol layers. The lowermost layer between 0.5 and 2 km causing a strong backscattered peak, is characterized by lidar ratios about 25 sr. By contrast, the upper layer between 2 and 6 km that we believe is mainly made of Sahara dust particles, is characterized by a backscatter coefficient of about 0.0016 $(\mathrm{km\ sr})^{-1}$ and by lidar ratio values of about 50 sr. The nearly adiabatic potential temperature profile between 2 and 5 km that is shown on Fig. 10a (dots), further supports the presence of a mixed layer within this vertical range. The aerosol optical thickness of this last layer computed by integrating the extinction profile between 2 and 6 km is 0.26. The larger values of the backscatter coefficients besides the smaller values of the lidar ratio below 2 km altitude, may be ascribed to a larger presence of marine aerosols. This last comment is further supported by the back trajectories of Fig. 7. For large, marine particles the lidar ratio is expected to be in the range 17-24 at 355 nm and between 19-28 sr at 532 nm in accordance to Ref. 25. By contrast, lidar ratios ranging from 10 to 60 sr at 532 nm have been provided by the numerical model developed by Barnaba and Gobbi [24]. The layer above about 5.5 km could also be due to Sahara dust accordingly to the back trajectories of Fig. 7 but, the rather small values of the extinction and backscatter coefficients besides their large relative statistical uncertainties do not allow a proper characterization of this layer.

## 4. Dust-sample characterization

Several dust samples have been collected by sedimentation at the lidar site during the dust event that started on May 17$^{th}$ in order to characterize the chemical and morphological properties of the collected particles[26] and further support the origin of the monitored aerosol layers. Moreover, there is a clear need to provide information on the dust mineralogical composition[27] needed for dust modeling on global and regional scales. The dust samples have been collected on glass substrates at about 5 m from ground and the typical sampling duration was of 6-8 hours. Care was taken to avoid the contamination by local sources as dust like particles both during the sampling duration and before the sample processing time. The samples have been processed few days after the collection day. However, it has been observed that the results on sample characterization were not dependent on the time elapsed between collection and processing.  We have examined the composition of these samples qualitatively by two methods. The first method was infrared transmission spectroscopy, using the conventional KBr pellet technique with a Perkin Elmer Spectrum 2000 FT-IR spectrometer in the 1.5-26 μm spectral region. To this purpose about 0.1% by mass of the dust taken away from the glass substrate has been embedded in 250 mg of powder of potassium bromide (KBr), which is transparent in the spectral range of interest. This method produces a transmittance spectrum that can provide qualitative information on the major chemical constituents in the sample. Several dust samples have been analyzed and it has been found that the transmittance spectrum was not dependent on the sample. A typical transmittance spectrum of the analyzed samples is shown in Fig. 11 (solid line). A comparison of this spectrum with an infrared spectral library of minerals[28], allows us to recognize that the collected dust contains a significant amount of illite $(K,H_3O)(Al,Mg,Fe)_2(Si,Al)_4O_{10}[(OH)_2,H_2O]$, that is a mineral classified as a phyllosilicate of the mica group, with absorption bands centered around 9.7 μm, 11.0 μm, 18.9 μm, 21.3 μm and 23.5 μm . The transmittance spectrum of illite taken from Ref. 28 is also shown in Fig. 11 (dotted line) for comparison. The contribution of some carbonate bands at 7 μm, 11.5 μm and 14 μm, and quartz bands at 9.3 μm, 12.5 μm, 18.9 μm and 21.3, can also be observed in the transmittance spectrum of Fig. 11 (solid line). The strong features clearly visible in Fig. 11 (solid line) around 2.9 μm and 6.1 μm, can be certainly ascribed to the O-H stretching vibrations and to the H-O-H bending vibrations of water, respectively. Let us mention that the strong absorption bands in the 8 – 12 μm atmospheric window, which are typical of desert aerosols, lead to an increase of the green-house effect in the thermal infrared (IR).

Several dust samples have in addition been examined by a field emission Scanning Electron Microscope (SEM Philips XL-20) equipped with an x-ray energy dispersive (EDX) system (EDAX DX-4), for their morphological characterization and elemental composition. For this analysis a suspension of dust particles and pure alcohol deposited on Si wafers has been used. The qualitative EDX elemental analysis reported in Fig. 12 can be considered as a confirmation of the identification of the materials made on the basis of the infrared spectroscopy measurements. Moreover, Fig. 12 reveals that the collected dust contains Na and Cl. In fact, during normal meteorological conditions, which are dominated by westerly flow, the aerosol samples are found to contain large amount of NaCl particles from the sea together with soil-type aerosols originating from the North African desert[27]. Finally, SEM images obtained at different magnifications have revealed that the shape of the grains, often clustered together, is quite irregular with a size which is generally smaller than 20 μm, in accordance to previously reported experimental results[5]. In conclusion, all these observations are consistent with the view that dust originating from the North African desert was collected at the lidar station. Let us mention that Sokolik and Toon have reported in Ref. 26, that the dust originating from Ahaggar Massif (Chad and Lybia) is characterized by a high abundance of illite, while the dust from the Tibesti Mountains (Egyptian, Libyan, and Negev deserts) has moderate concentrations of illite, kaolinite and montmorillonite. To this end, it is worth observing that Fig. 7 reveals that the region close to Ahaggar Massif is the main source area of the back trajectories reaching Lecce on May 17th.

## 5. Conclusion

Results on the optical characterization of dust layers monitored by an elastic-Raman lidar in the south-eastern corner of Italy during May 2001, have been reported. Strong Sahara dust events generally happen every year over the Mediterranean regions during the month of May[5], and two severe African dust outbreaks with dust clouds characterized by a quite different vertical structure and temporal evolution have been monitored on May, 2001. A direct documentation on the vertical structure of the dust layer is of peculiar importance to infer their radiative impact[1,3,4]. A dust layer of thickness ranging from about 1 to 3 km and located above 3 km height has been monitored during May 3rd and 4th. The peak values of the backscatter coefficient were in the range 0.001- 0.003 (km sr)$^{-1}$ and the AOT of the dust layer monitored between 3 and 6 km on the late night of May 3rd was of 0.21. By contrast, a dust layer extending between 2.7 and 5.4 km and characterized by an AOT of 0.22 has been monitored on May 4th between the 22:01 and the 23:02 UT. Average lidar ratio values of 55 sr have been found during this first dust event.

A dust layer of thickness ranging between 4 and 5 km has been monitored at heights above 1 km, during the last African dust event. Average lidar ratio values of 50 sr have been found during this last event, in satisfactory accordance with previous measurements and numerical values. It has also been found that the peak values of the aerosol backscatter coefficient vary between 0.002 and 0.005 $(km\ sr)^{-1}$ and that the dust layer monitored on May $17^{th}$ at 19:30 between 2 and 6 km is characterized by an optical depth of 0.26. Finally, the chemical characterization of the dust samples collected during the dust event of May $17^{th}$, has allowed us to recognize that the collected dust contains a significant amount of illite besides carbonates, quartz, water and, particles of NaCl from the sea, in accordance to previously reported analysis.

In conclusion, the main aim of the paper was to discuss lidar data sets that are representative of Sahara dust outbreaks happening over the Mediterranean regions. It is believed that the data presented may help scientists to understand, describe and forecast Sahara dust characteristics and effects over the Mediterranean area.

**Acknowledgments**

This work has been supported by the Environment Program of the European Union, under the contract No. EVR1-CT1999-40003. The air-mass back trajectories analysis was performed by the German Weather Service, by using the Interactive Data Analysis code (IDL) code provided by I. Mattis (Institut fur Tropospharenforschung, leipzig, Germany). The radiosounding data of the Meteorological Station of Brindisi (Italy) have been provided by NOAA (http://raob.fsl.noaa.gov). The authors would like to thank the SeaWiFS Project (Code 970.2) and the Goddard Earth Sciences Data and Information Services Center/Distributed Active Archive Center (Code 902) at the Goddard Space Flight Center, Greenbelt, MD 20771, for the production and distribution of these data, respectively. These activities are sponsored by NASA's Earth Science Enterprise.

## References


1. E. Hamonou, P. Chazette, D. Balis, F. Dulac, X. Schneider, E. Galani, G. Ancellet, and A. Papayannis, “Characterization of the vertical structure of Saharan dust export to the Mediterranean basin, “ J. of Geophys. Res. **104**, 22257-22270 (1999).
2. G. P. Gobbi, F. Barnaba, R. Giorgi, and A. Santacasa, “Altitude-resolved properties of a Sahara dust event over the Mediterranean,” Atmosph. Envir. **34**, 5119-5127 (2000).
3. I. Sokolik and O. B. Toon, “Direct radiative forcing by anthropogenic airborne mineral aerosols,” Nature, **381**, 681-683 (1996)’
4. I. Tegen and I. Fung, “ Contribution to the atmospheric mineral aerosol load from land surface modification,” J. of Geophys. Res., **100**, 18707-18726 (1995).
5. F. Prodi and G. Fea, “A case of transport and deposition of Sahara dust over the Italian peninsula and southern Europe,” J. of Geophys. Res. **84**, 6951-6960 (1979).
6. I. Mattis, A. Ansmann, D. Muller, U. Wandinger, and D. Althausen, “Dual-wavelength Raman lidar observations of the extinction-to-backscatter ratio of Sahara dust,” Geophys. Res. Lett., **29** (2002).
7. A. Ansman, M. Riebesell, U. Wandinger, C. Weitkamp, E. Voss, W. Lahmann, and W. Michaelis, “ Combined Raman elastic-backscatter LIDAR for vertical profiling of moisture, aerosol extinction, backscatter, and lidar ratio, “ Appl. Phys. **B55**, 18-28 (1992).
8. S. B. Hooker, W. Esaias, G. Feldman, W. Gregg, and C. R. McClain, SeaWiFS Technical Report Series: vol. 1 “An Overview of the SeaWiFS and Ocean Color”, NASA Techn. Memo. 104566 (NASA Greenbelt Space Center, Greenbelt, Md., July 1992).
9. J. Bosenberg, A. Ansmann, J. Baldasano, D. Balis, C. Bockmann, B. Calpini, A. Chaikovsky, P. Flamant, A. Hagard, V. Mitev, A. Papayannis, J. Pelon, D. Resendes, J. Schneider, N. Spinelli, T. T, G. Vaughan, G. Visconti, and M. Wiegner, “EARLINET: A European aerosol research lidar network,” In *Laser Remote Sensing of the Atmosphere. Selected papers of the*

*20th International Laser Radar Conference,* A. Dabas, C. Loth, and J. Pelon (Eds.), 155-158 (2000). Edition Ecole Polytechnique, Palaiseau (France).

10. A. Ansmann, U. Wandinger, M. Riebesell, C. Weitkamp, and W. Michaelis, “Independent measurement of extinction and backscatter profiles in cirrus clouds by using a combined Raman elastic-backscatter lidar,” Appl. Opt. **31**,7113-7131 (1992).
11. R. A. Ferrare, S. H. Melfi, D. N. Whiteman, K. D. Evans, and R. Leifer, “Raman lidar measurements of aerosol extinction and backscattering. 1. Methods and comparisons” J. Geophys. Res., **103**, 19663-19672 (1998).
12. A. Ansmann, M. Riebesell, and C. Weitkamp, “Measurements of atmospheric aerosol extinction profiles with a Raman Lidar”, Optics Lett. **15**, 746-748 (1990).
13. F. G. Fernald, “Analysis of atmospheric lidar observations: some comments ”, Appl. Opt. **23**, 652-653 (1984).
14. V. Matthias et al., “ Lidar intercomparison on algorithm and system level in the frame of EARLINET ”, Max-Plank-Institute fur Meteorologie, Report No. 337.

    V. Freudenthaler et al., “ Intercomparison of 21 aerosol lidar system in the frame of EARLINET ”, in “Lidar Remote Sensing in Atmosphere and Earth Sciences”, proceedings of the XXI International Laser Radar Conference, Quebec, Canada, 8-12 July 2002, L.R. Bissonette, G. Roy, and G. Valle editors.
15. C. Kottmeier and B. Fay, “Trajectories in the antarctic lower troposphere,” J. Geophys. Res. **105**, 10947-10959 (1998).
16. A. Stohl, “Computation, accuracy and application of trajectories- a review and bibliography,” Atmos. Environ., **32**, 947-966 (1998).
17. J. Bosenberg, “EARLINET: A European Aerosol Research Lidar Network to Establish an aerosol Climatology”, Contract EVR1-CT1999-40003. Scientific Report for the period February 2001 to January 2002 (March 2002).

18. P. B. Russell, T. J. Swissler, and M. P. McCormick, “Methodology for error analysis and simulation of lidar aerosol measurements,” Appl. Opt., **18**, 3783-3797 (1979).

19. A. Ansmann, F. Wagner, D. Althausen, D. Muller, A. Herber, and U. Wandinger, “Pollution Outbreaks During ACE2, Part I: Alofted Aerosol Plumes observed with Raman Lidar at the Portuguese Coast”, J. Geophys. Res. **106 D**, 20723-20733 (2001).

20. A. Ansmann, D. Althausen, U. Wandinger, K. Franke, D. Muller, F. Wagner, and J. Heintzenberg, “Vertical profiling of the Indian aerosol plume with six-wavelength lidar during INDOEX: A first case study,” Geophys. Res. Lett., **27**, 963-966 (2000).

21. R. A. Ferrare, S. H. Melfi, D. N. Whiteman, K. D. Evans, and R. Leifer, “Raman lidar measurements of aerosol extinction and backscattering. 1. Methods and comparisons,” J. Geophys. Res., **103**, 19663-19673 (1998).

22. R. A. Ferrare, D. D. Turner, L. H. Brasseur, W. F. Feltz, O. Dubovik, and Tim Tooman, “Raman lidar measurements of the aerosol extinction-to-backscatter ratio over the Southern Great Plains,” J. Geophys. Res., **106**, 20333-20347 (2001).

23. Y. Sasano and E. V. Browell, “Light scattering characteristics of various aerosol types derived from multiple wavelength lidar observations,” Appl. Optics **28**, 1670-1679 (1989).

24. F. Barnaba and G. P. Gobbi, “Lidar estimation of tropospheric aerosol extinction, surface area and volume:Maritime and desert-dust cases,” J. of Geophys. Res.,**106**, 3005-3018 (2001).

25. J. Ackermann, “The extinction-to-backscatter ratio of tropospheric aerosol: a numerical study,” J. of Atm. and Oceanic Techn., **15**, 1044-1050 (1998).

26. Z. Levin and J. D. Lindberg, “Size distribution, chemical composition, and optical properties of Urban and desert aerosols in Israel,” J. of Geophys. Res. **84**, 6941-6950 (1979).

27. I. N. Sokolik and O. B. Toon, “Incorporation of mineralogical composition into models of the radiative properties of mineral aerosol from UV to IR wavelenth,” J. of Geophys. Res. **104**, 9423-9444 (1999).

28. J. W. Salisbury, L. S. Walter, N. Vergo, and D. M. D' Aria, Infrared (2.1 - 25 μm) Spectra of Minerals, John Hopkins University Press, Baltimore/London (1991).

**Figure Captions**

Fig. 1 Experimental layout of the XeF-based Rayleigh-Raman lidar operating at the University of Lecce (40° 20’ N, 18° 6’ E). A, field stop aperture; L’s, lenses; Q, uncoated fused silica plate; F, neutral density filters; Mn’s, monochromators; Ph’s, photosensors; MCS’s, multichannel scalers; Disc’s, discriminators.

Fig.2 Four-day back trajectories for air parcels arriving over the lidar station of Lecce on May 3$^{rd}$ at 13:00 UT.

Fig. 3 SeaWiFS image taken on May 4$^{th}$ over the Eastern Mediterranean Sea and Southern Italy.

Fig. 4 Average profiles of the aerosol backscatter coefficient measured at different hours of the day on (a) May 3$^{rd}$ and (b) May 4$^{th}$. The measurement time (UT) is reported on the right side of each profile.

Fig.5 Average profiles of (a) the aerosol backscatter coefficient, (b) the aerosol extinction coefficient and (c) the lidar ratio retrieved from measurements started on May 3$^{rd}$ at 23:40 UT and ended on May 4$^{th}$ at 01:00 UT. The backscatter coefficient profile is smoothed with an average window length of 60 m. Error bars indicate one standard deviation caused by statistical uncertainties and have been calculated from the law of error propagation by assuming a Poisson noise on lidar signals. The extinction profile is calculated by a linear fit of the logarithm of the Raman signal as explained in the text. The error bars are one standard deviation in the slope of the fitting straight line. The fitting intervals are 150 and 300 m below and above 1.2 km height, respectively. The potential temperature profile obtained from radiosonde measurements performed at Brindisi on May 3$^{rd}$ at 23:00 UT is shown by full dots in (a).

Fig. 6 Average profiles of the aerosol (a) backscatter coefficient, (b) extinction coefficient and, (c) the lidar ratio measured on May 4$^{th}$ from 22:00 to 23:00 UT. The backscatter coefficient profile is smoothed with an average window length of 60 m. The extinction profile is calculated by a linear fit of the logarithm of the Raman signal as explained in the text. The fitting intervals are 150 and 450 m below and above 1.2 km height, respectively. The error bars are one standard deviation in the slope of the fitting straight line. The potential temperature profile obtained from radiosonde measurements performed at Brindisi on May 4th at 23:00 UT is shown by full dots in (a).

Fig. 7 Four-day back trajectories for air parcels arriving over the lidar station of Lecce on May 17th at 19:00 UT.

Fig. 8 SeaWiFS image taken on May 18th over the Eastern Mediterranean Sea, Southern Italy and Greece.

Fig. 9 Average profiles of the aerosol backscatter coefficient measured on several days of May, 2001. The day and measurement time (UT) are reported on the right side of each profile.

Fig.10 Average profiles of the aerosol (a) backscatter coefficient, (b) extinction coefficient and, (c) lidar ratio measured on May 17th from 18:55 to 20:07 UT. The backscatter coefficient profile is smoothed with a sliding average length of 60 m and 120 m below and above 6 km. The fitting intervals of the extinction profile are 150 and 450 m below and above 1.2 km height, respectively. The potential temperature profile obtained from radiosonde measurements performed at Brindisi on May 17th at 23:00 UT is shown by full dots in (a).

Fig.11 Typical infrared potassium bromide pellet transmission spectrum of dust samples that have been collected at the lidar station during the dust event of May 17th (solid line). The dotted line is the transmission spectrum of illite taken from Ref. 27.

Fig. 12 Typical EDX elemental analysis of the dust samples.

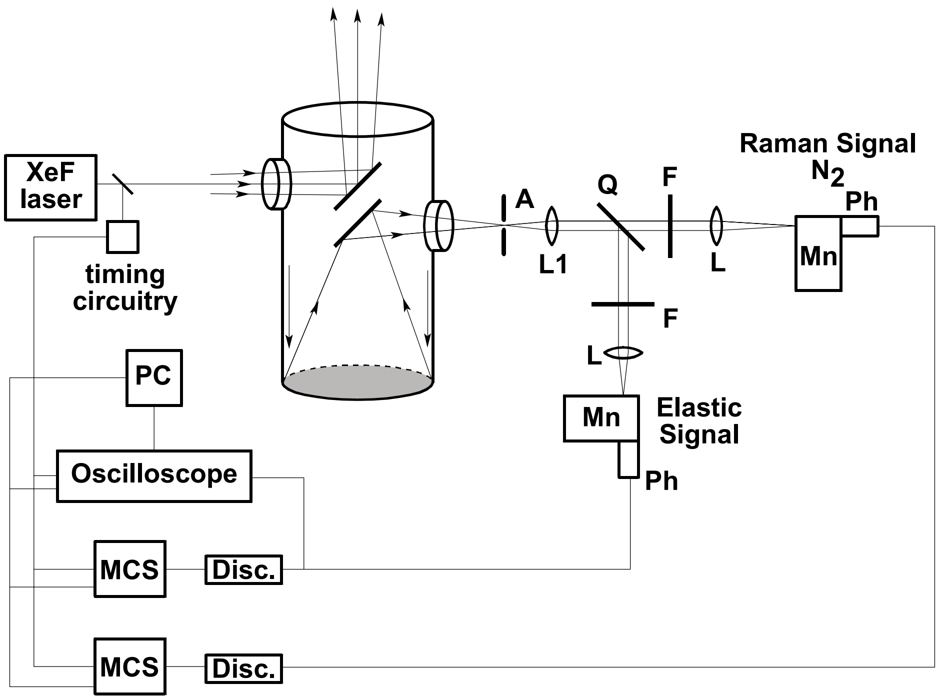

XeF laser
timing circuitry
PC
Oscilloscope
MCS
Disc.
MCS
Disc.
A
L1
Q
F
L
Raman Signal
$N_2$
Ph
Mn
F
L
Mn
Elastic Signal
Ph

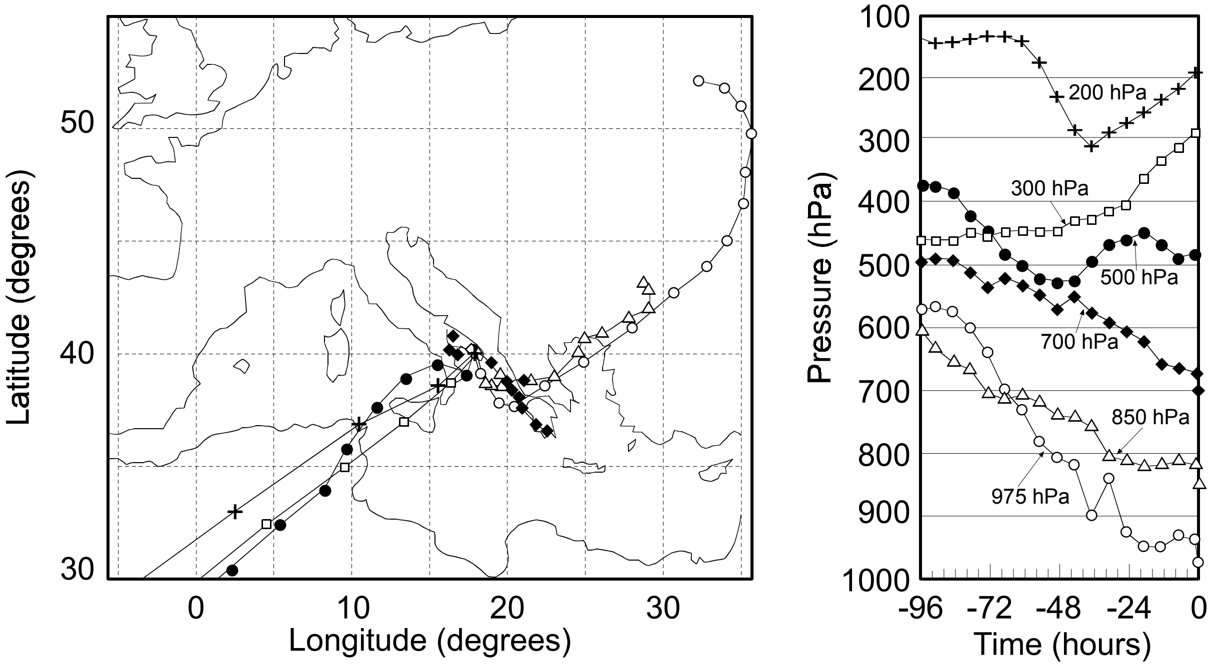

Latitude (degrees)
50
40
30
0
10
20
30
Longitude (degrees)
Pressure (hPa)
100
200
300
400
500
600
700
800
900
1000
200 hPa
300 hPa
500 hPa
700 hPa
850 hPa
975 hPa
-96
-72
-48
-24
0
Time (hours)

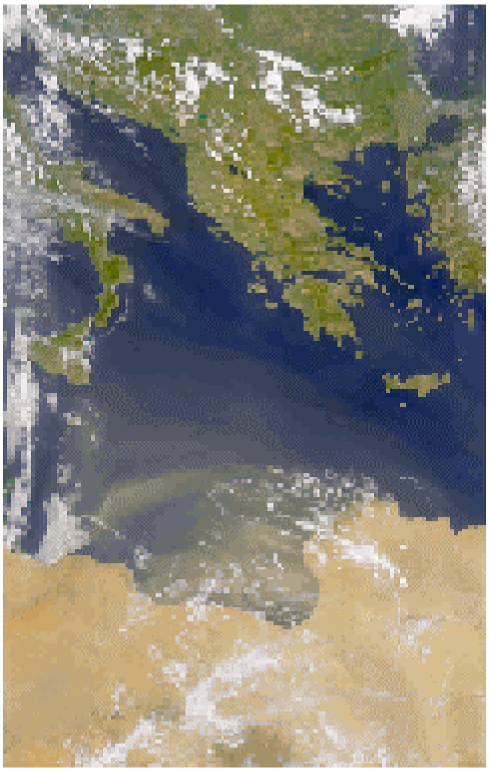

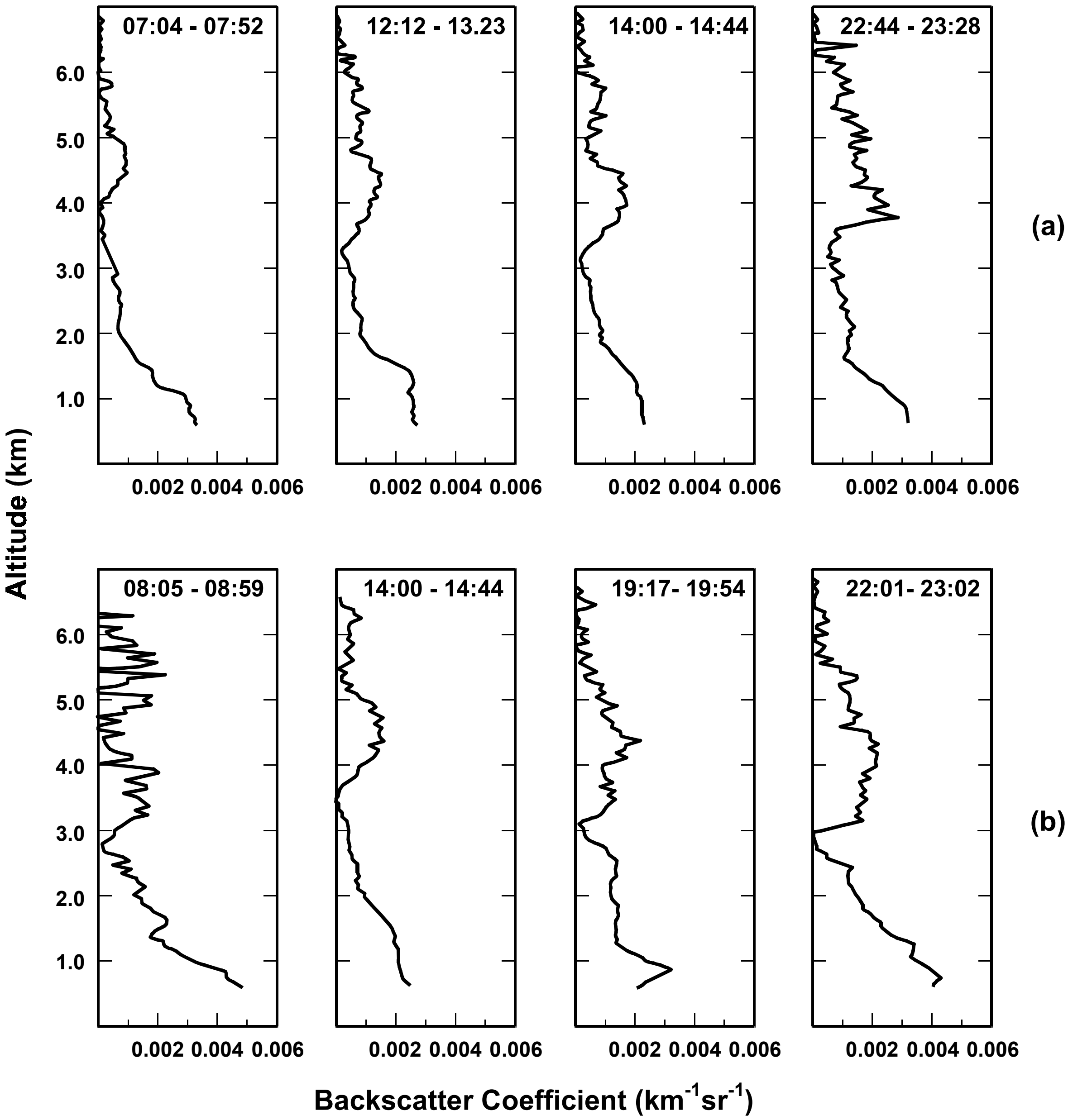
07:04 - 07:52
12:12 - 13.23
14:00 - 14:44
22:44 - 23:28
08:05 - 08:59
14:00 - 14:44
19:17- 19:54
22:01- 23:02
(a)
(b)
Altitude (km)
1.0
2.0
3.0
4.0
5.0
6.0
0.002 0.004 0.006
Backscatter Coefficient (km-1sr-1)

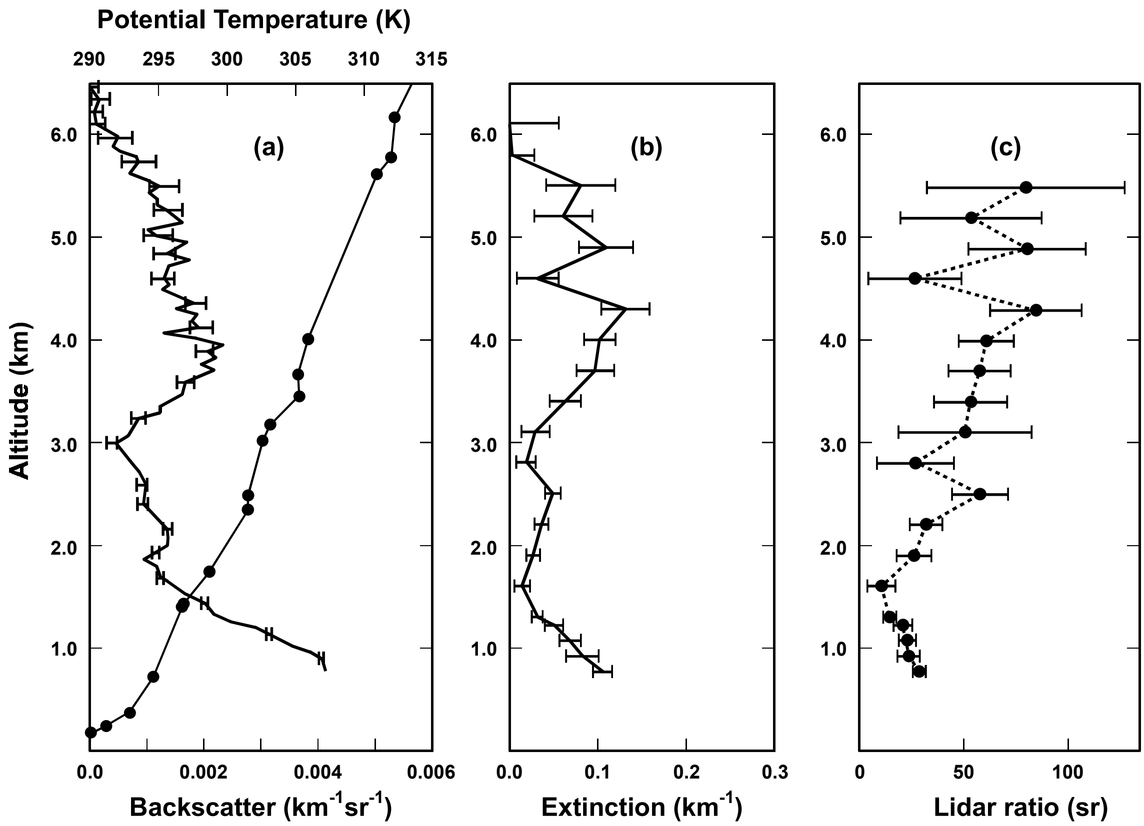

Potential Temperature (K)
290
295
300
305
310
315
(a)
(b)
(c)
6.0
5.0
4.0
3.0
2.0
1.0
Altitude (km)
0.0
0.002
0.004
0.006
Backscatter (km-1sr-1)
0.0
0.1
0.2
0.3
Extinction (km-1)
0
50
100
Lidar ratio (sr)

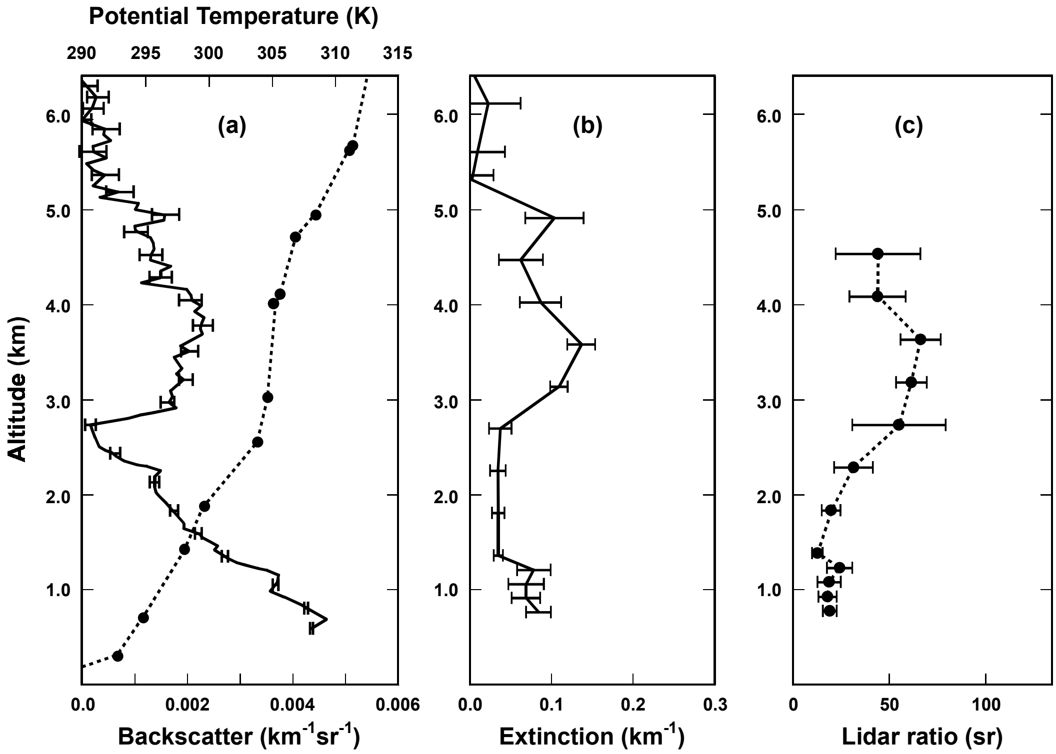
Potential Temperature (K)
290
295
300
305
310
315
Altitude (km)
6.0
5.0
4.0
3.0
2.0
1.0
(a)
(b)
(c)
0.0
0.002
0.004
0.006
Backscatter (km-1sr-1)
0.0
0.1
0.2
0.3
Extinction (km-1)
0
50
100
Lidar ratio (sr)

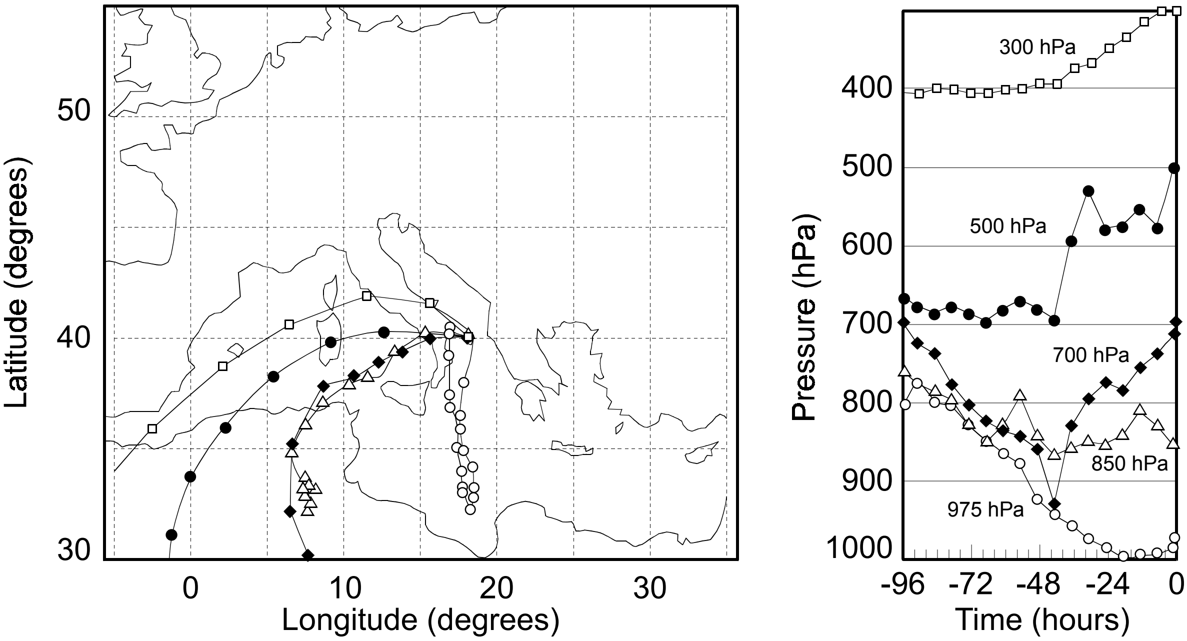

Latitude (degrees)
Longitude (degrees)
50
40
30
0
10
20
30
Pressure (hPa)
Time (hours)
300 hPa
500 hPa
700 hPa
850 hPa
975 hPa
400
500
600
700
800
900
1000
-96
-72
-48
-24
0

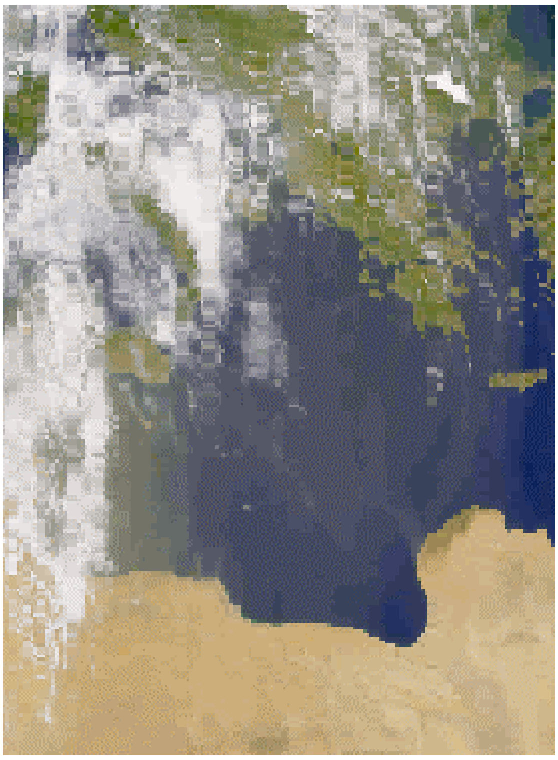

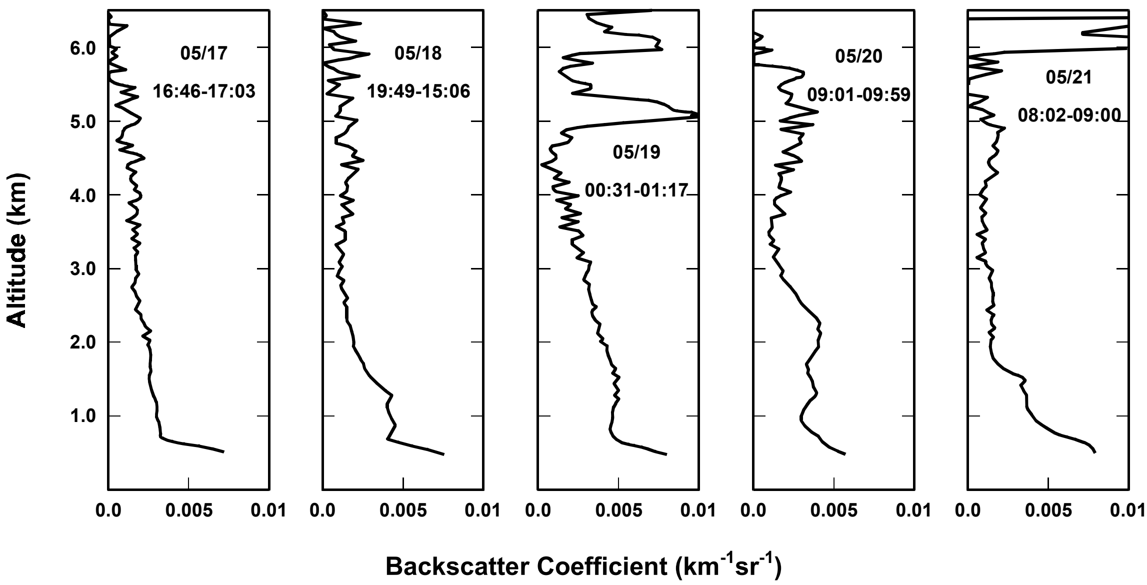
Altitude (km)
6.0
5.0
4.0
3.0
2.0
1.0
05/17
16:46-17:03
05/18
19:49-15:06
05/19
00:31-01:17
05/20
09:01-09:59
05/21
08:02-09:00
0.0
0.005
0.01
Backscatter Coefficient (km-1sr-1)

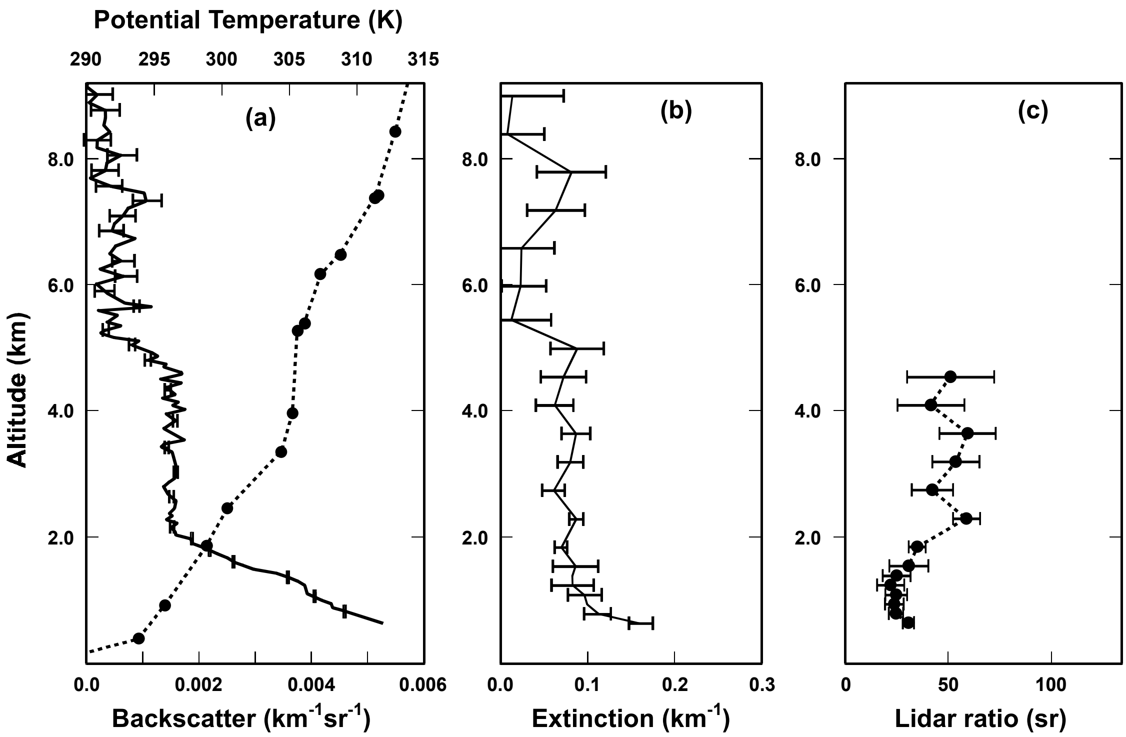
Potential Temperature (K)
290
295
300
305
310
315
(a)
(b)
(c)
8.0
6.0
4.0
2.0
Altitude (km)
0.0
0.002
0.004
0.006
Backscatter (km-1sr-1)
0.0
0.1
0.2
0.3
Extinction (km-1)
0
50
100
Lidar ratio (sr)

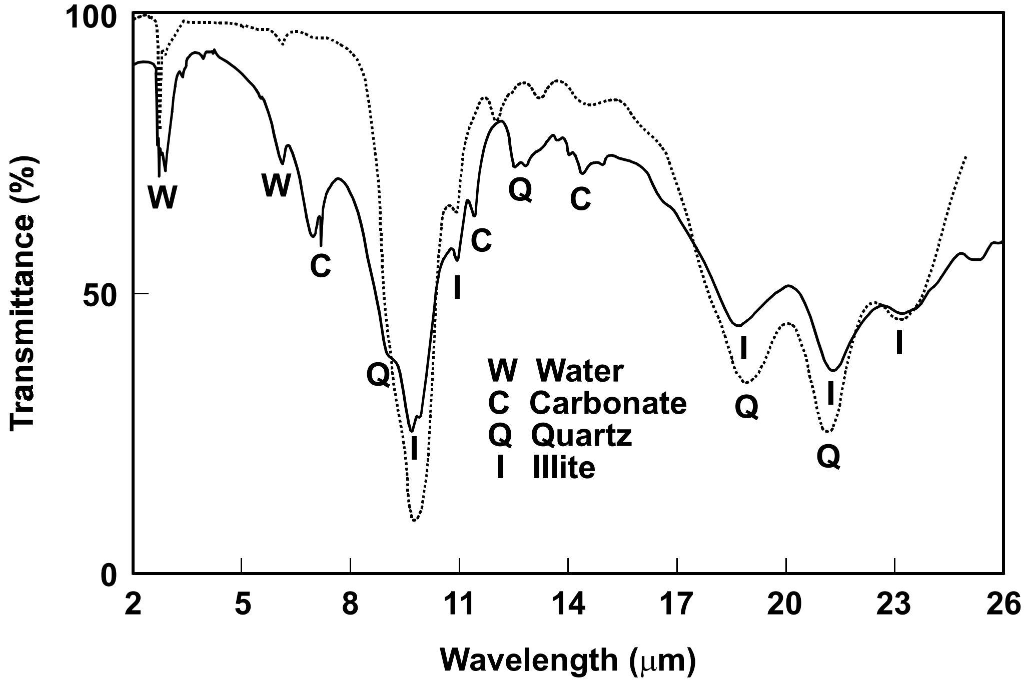

Transmittance (%)
100
50
0
2
5
8
11
14
17
20
23
26
Wavelength (μm)
W
W
C
Q
I
I
C
Q
C
I
Q
I
Q
I
W Water
C Carbonate
Q Quartz
I Illite

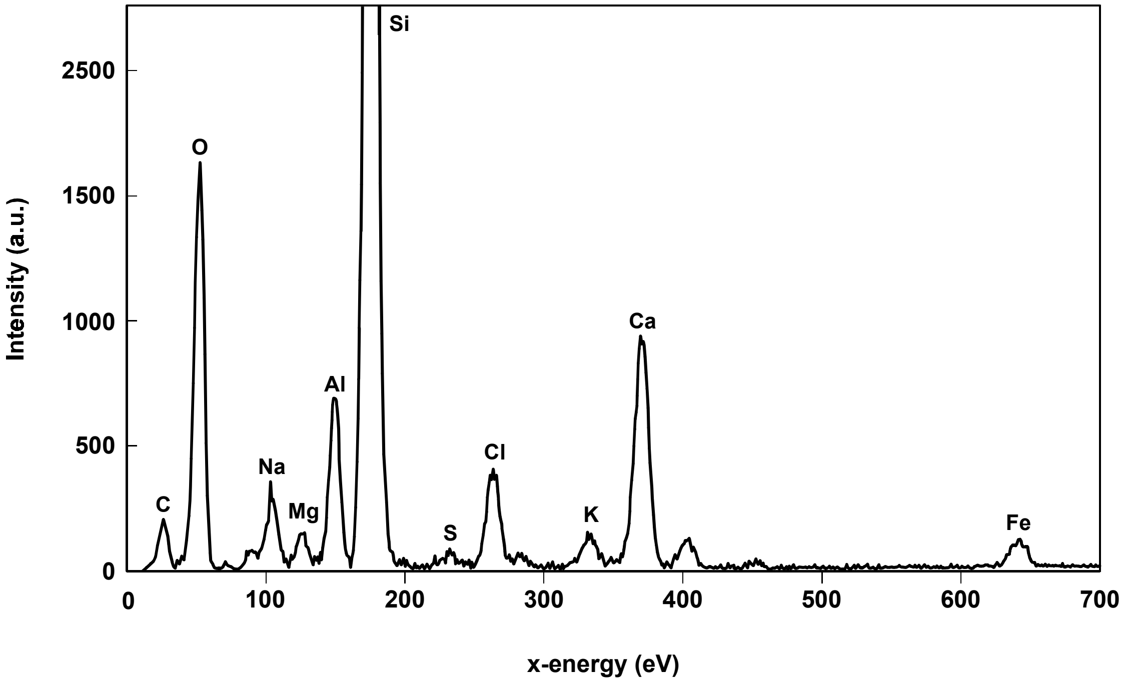
Intensity (a.u.)
x-energy (eV)
0
500
1000
1500
2500
0
100
200
300
400
500
600
700
C
O
Na
Mg
Al
Si
S
Cl
K
Ca
Fe